Three-octave-spanning supercontinuum generation and sub-two-cycle self-compression of mid-infrared filaments in dielectrics

Houkun Liang,[1] Peter Krogen,[1] Ross Grynko,[2] Ondrej Novak,[1] Chun-Lin Chang,[1] Gregory J. Stein,[1] Darshana Weerawarne,[2] Bonggu Shim,[2] Franz X. Kärtner,[1,3,4] and Kyung-Han Hong[1,*]

[1]*Department of Electrical Engineering and Computer Science and Research Laboratory of Electronics, Massachusetts Institute of Technology (MIT), Cambridge, Massachusetts 02139, USA*

[2]*Department of Physics, Applied Physics and Astronomy, Binghamton University, State University of New York, Binghamton, New York 13902, USA*

[3]*Center for Free-Electron Laser Science, DESY and Department of Physics, University of Hamburg, Hamburg, Germany*

[4]*The Hamburg Center for Ultrafast Imaging, Luruper Chaussee 149, 22761 Hamburg, Germany*

**Corresponding author: kyunghan@mit.edu*

Received December 12, 2014; revised February 6, 2015; accepted February 7, 2015; posted February 10, 2015 (Doc. ID 230611); published March 11, 2015

We experimentally and numerically investigate the spectral and temporal structure of mid-infrared (mid-IR) filaments in bulk dielectrics with normal and anomalous group velocity dispersion (GVD) pumped by a 2.1 μm optical parametric chirped-pulse amplifier (OPCPA). The formation of stable and robust filaments with several microjoules of pulse energy is observed. We demonstrate a supercontinuum that spans more than three octaves from ZnS in the normal GVD regime and self-compression of the mid-IR pulse to sub-two-cycle duration in CaF_2 in the anomalous GVD regime. The experimental observations quantitatively agree well with the numerical simulations based on a three-dimensional nonlinear wave equation that reveals the detailed spatio-temporal dynamics of mid-IR filaments in dielectrics.

OCIS codes: (320.6629) Supercontinuum generation; (320.7110) Ultrafast nonlinear optics; (320.5520) Pulse compression.

http://dx.doi.org/10.1364/OL.40.001069

Supercontinuum generation (SCG) has attracted extensive attention owing to its broad applications in sensing, spectroscopy, optical coherence tomography, and so on [1]. Extending SCG to the mid-infrared (mid-IR) range is highly desirable for detecting biomedical materials and air pollutants with the resonant fingerprints of the most common molecules, such as H_2O, CO_2, CO, and NH_4. Moreover, coherent broadband mid-IR supercontinuum (SC) is a good candidate to be the seed of mid-IR optical parametric amplifiers (OPAs) and optical parametric chirped-pulse amplifiers (OPCPAs) for strong-field physics and attosecond science. In general, high-energy, few-cycle mid-IR pulses are extremely useful for the time-resolved studies of the fundamental processes in physics and chemistry.

The research work on SCG and pulse compression in the mid-IR range in the past decade has mostly explored SCG in fibers [2–5] and high-pressure noble gases [6]. SCG covering the whole mid-IR "fingerprint region" was demonstrated very recently in a chalcogenide step-index fiber pumped by 4.5 and 6.3 μm lasers [7]. However, there are intrinsic peak power limitations and alignment sensitivity issues that come with the method of fiber-based SCG. Recently, the advantages of filamentation in bulk dielectrics [8–10] presented new opportunities. These advantages include flexible materials available in the normal and anomalous group velocity dispersion (GVD) regimes, no limitation of confinement loss at long wavelengths, a highly adaptable pump power, and high throughput. Moreover, the feasibility of few-cycle self-compression has been studied in bulk dielectrics with anomalous GVD pumped by femtosecond optical pulses at 1.8 [11], 1.9 [12], and 3.1 μm [13].

In this Letter, we use a pump wavelength of 2.1 μm, generated from an OPCPA, for laser filamentation [14] in the mid-IR regime. This wavelength is compatible to the recently developed ultrafast laser amplifiers based on thulium- or holmium-doped materials [15]. We systematically investigate mid-IR SCG from filaments in different dielectrics in both the normal and anomalous GVD regimes. A more than three-octave broadband spectrum is demonstrated for the first time in ZnS in the normal GVD regime. Moreover, mid-IR pulse self-compression down to a sub-two-cycle duration is demonstrated in CaF_2 in the anomalous GVD regime. Up to 9 μJ of pulse energy from the SC has been generated.

For a systematic study of SCG in the mid-IR, CaF_2 (5 mm thick), BaF_2 (6 mm thick), and ZnS (8 mm thick), all of which have a relatively flat dispersion around 2 μm, were chosen as the bulk dielectric materials. The zero-dispersion wavelength of the three materials is 1.67, 1.92, and 3.6 μm, respectively, as shown in Fig. 1(a). The bulk dielectrics were pumped by a 2.1 μm, 27 fs, 1 kHz OPCPA with passive carrier-envelope phase stabilization [16]. The pump-pulse energy was varied in the range from 0.1 to 11 μJ for the optimization of the SCG process towards an ultra-broad bandwidth and stable single filamentation. The pump beam was focused using an $f = 100$ mm CaF_2 lens to a $1/e^2$ diameter of ~200 μm. We placed the input surface of the dielectrics 4–7 mm before the focal spot to (1) enable the end of the filament to be just at the output surface of the dielectrics; and (2) avoid focusing on the dielectric surface,

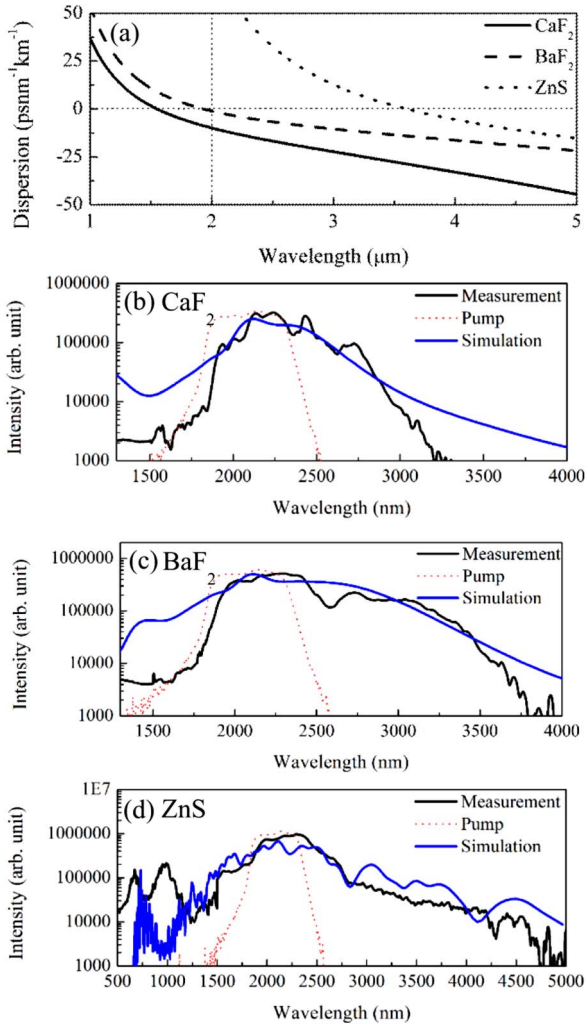

Fig. 1. (a) Material dispersion of CaF_2 (solid black line), BaF_2 (dashed black line), and ZnS (dotted black line). The measured (black line) and simulated (blue line) spectrum of the generated SC from the 5 mm-thick CaF_2 at 9 μJ (b), the 6 mm-thick BaF_2 at 7 μJ (c), and the 8 mm-thick ZnS at 5 μJ (d). The dotted curves in (b), (c), and (d) are the spectra of the 2.1 μm pump laser.

thereby causing damage. Three different spectrometers, based on Si, InGaAs, and PbSe detectors, were employed to cover the spectra spanning from the visible wavelength to a wavelength of ~5 μm.

As shown in Figs. 1(b) and 1(c), with the pump wavelength at 2.1 μm, the continuum spectrum is extended to wavelengths of up to ~3.3 and ~3.8 μm in CaF_2 and BaF_2, respectively. The deeper extension into the mid-IR in BaF_2 is due to its flatter and lower dispersion, and thus broader conversion bandwidth with less temporal walk-off. Moreover, we performed SCG in a ZnS crystal with a normal GVD for the first time. As shown in Fig. 1(d), the generated SC spans from 500 to 4.5 μm, corresponding to 3.1 octaves. The peaks at ~980 and ~670 nm are observed where the 670 nm component is possibly the third harmonic of the 2.1 μm pump pulse. It is interesting to note that ZnS has a nonlinear refractive index (n_2) as high as 90×10^{-16} cm^2/W, which is ~50 times larger than that of CaF_2. Surprisingly, we were still able to maintain a very stable filament with an input energy of 11 μJ, which corresponds to ~1000 times the critical power for self-focusing. The normal GVD seems to help the stable filamentation at an over-critical power by rapidly broadening the pulse, but further investigation is needed to understand the details of the mechanism.

The visible images of the far-field pattern and the filaments inside CaF_2, BaF_2, and ZnS are captured. Stable conical far-field profiles were observed for SC from CaF_2 and BaF_2, as shown in Figs. 2(a) and 2(b), while ZnS has a more uniform far-field pattern, as shown in Fig. 2(c). The filaments from all three dielectrics manifest a robust single filament, as shown in Figs. 2(d)–2(f).

The temporal profiles of the generated mid-IR SC were characterized using a second-harmonic generation (SHG) frequency-resolved optical gating (FROG) technique. A 100 μm thick β-BaB_2O_4 (BBO) and a 140 μm thick $AgGaS_2$ were used for the SHG of the pump pulse and the mid-IR filaments, respectively. The measured and retrieved FROG traces of the input pulse are shown in Fig. 3(a), while those from the SC in CaF_2 at different pump energies are shown in Figs. 3(b) and 3(c). The retrieved temporal and spectral profiles are shown in Figs. 3(d)–3(i). The pump pulse duration is 27 fs in full width at half maximum (FWHM), as shown in Fig. 3(d). For the SC in CaF_2, pumped at 6 μJ, the spectrum significantly extends to ~2.7 μm in linear scale, as shown in Fig. 3(g). A clear, tilted pulse shape with a steep trailing edge and a soft leading edge is revealed in Fig. 3(f). This shape is attributed to self-steepening. The retrieved pulse duration in FWHM is 19 fs. As the pump energy is further increased to 8.5 μJ, the spectrum of the SC further extends to ~2.9 μm in linear scale, as shown in Fig. 3(i). The pulse is further compressed to 13.5 fs in FWHM, as seen in Fig. 3(h) corresponding to ~1.8 cycles, at a ~2.25 μm central wavelength, while a few small pedestals emerge. The main pulse is close to transform limited because of the balance between self-phase modulation (SPM) and anomalous GVD. As for the SC in BaF_2, the retrieved pulse width is ~23 fs in FWHM, as shown in Fig. 3(k) retrieved from its FROG trace of Fig. 3(j). This indicates that the SPM-induced chirp has not been well compensated for by the weak anomalous GVD,

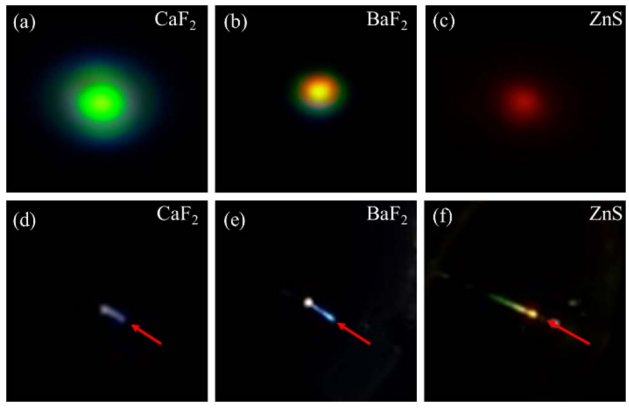

Fig. 2. Far field of the SC from (a) CaF_2, (b) BaF_2, and (c) ZnS. (d), (e), and (f) are the visible images of their corresponding filaments inside the material, respectively. The red arrows indicate the incident direction of the pump pulses.

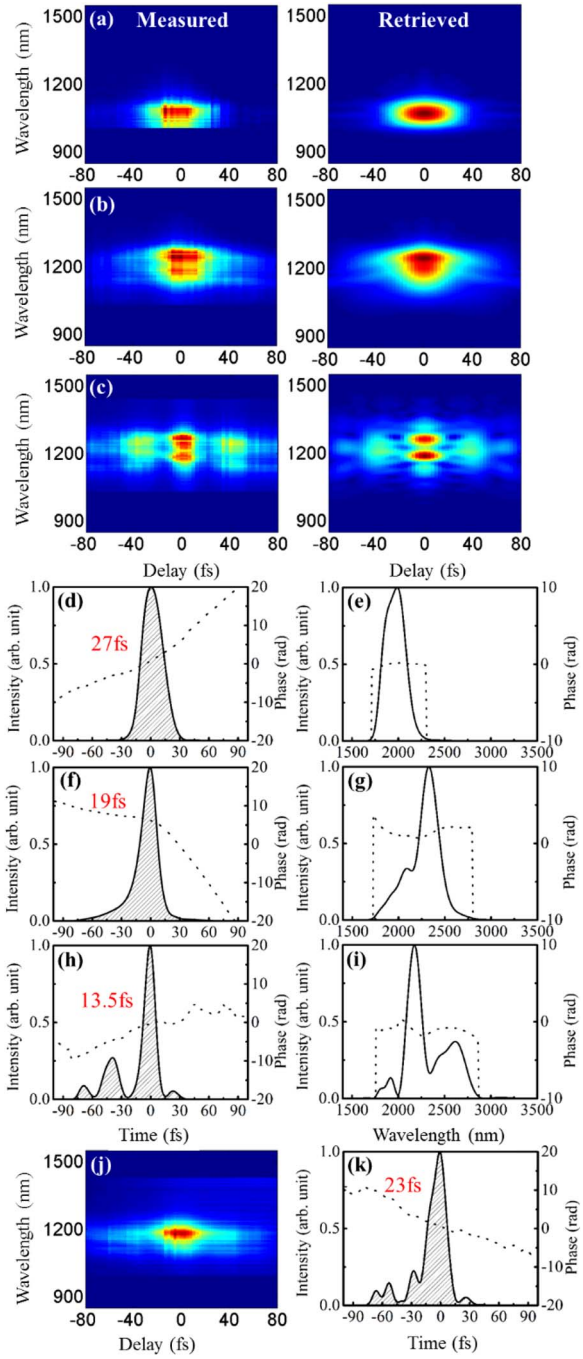

Fig. 3. Temporal characterization of mid-IR pulses using SHG FROG measurements. Measured and retrieved FROG traces of the pump pulse (a), the SC in CaF_2 pumped at 6 μJ (b), and the SC in CaF_2 pumped at 8.5 μJ (c). Retrieved intensity (solid line with gray stripe) and phase (dotted line) profiles of the pump pulses (d), the SC in CaF_2 at 6 μJ (f), and the SC in CaF_2 at 8.5 μJ (h). Retrieved spectrum (solid line) and spectral phase (dotted line) of the pump pulse (e), the SC in CaF_2 at 6 μJ (g), and the SC in CaF_2 at 8.5 μJ (i). The measured FROG trace of the SC in BaF_2 pumped at 6 μJ (j) and the retrieved intensity (solid line with gray stripe) and phase (dotted line) profiles (k).

compared to the CaF_2 case. On the other hand, the measured duration of the pulses from the ZnS filaments, which is not shown here, is longer than 200 fs because the SC forms the dispersive wave.

To gain a more quantitative understanding about the experiments, we carried out numerical simulations using the nonlinear envelope equation (NEE) in normalized units, which is given by [17,18]

$$\frac{\partial A}{\partial \xi} = \frac{i}{4}\left(1+\frac{i\partial}{\omega\tau_p\partial\tau}\right)^{-1}\nabla^2 A + iL_{df}\sum_{n=2}^{6}\frac{\beta_n}{n!}\left(\frac{i\partial}{\tau_p\partial\tau}\right)^n A + i\left(1+\frac{i\partial}{\omega\tau_p\partial\tau}\right)\frac{L_{df}}{L_{nl}}|A|^2 A - \frac{L_{df}}{2L_{mp}}\frac{A}{|A|^2}\frac{\partial\eta}{\partial\tau} - \frac{L_{df}}{L_{pl}}\left(i+\frac{1}{\omega\tau_c}\right)\eta\left(A+\frac{\frac{\tau_c\partial A}{\tau_p\partial\tau}}{1-i\omega\tau_p}\right), \quad (1)$$

where A is the electric field normalized by the input electric field amplitude, ξ is the propagation distance normalized by the input beam diffraction length L_{df}, and ω is the central frequency of the laser pulse. τ is the retarded time normalized by the pulse duration τ_p, β_n is the dispersion parameter (e.g., β_2 is GVD), L_{nl} is the nonlinear length, and L_{mp} is the multi-photon absorption length. L_{pl} is the plasma length, η is the normalized electron density, and τ_c is the collision time. Each term on the right side of the equation represents diffraction, dispersion, self-focusing via Kerr nonlinearity, multi-photon absorption, and plasma terms (defocusing and collisional absorption), respectively. Multi-photon ionization and avalanche ionization generate free electrons, which is described by

$$\frac{\partial\eta}{\partial\tau} = |A|^{2m} + \alpha\eta|A|^2, \quad (2)$$

where m is the number of photons needed to ionize the medium, and α is the avalanche ionization coefficient.

The simulated SCG reproduces the experimental measurements with high accuracy, as shown in Figs. 1(b)–1(d). The calculated output spectrum for BaF_2 has larger spectral components at 3–4 μm than that of CaF_2, which is consistent with the experimental data. For ZnS, the calculation also quantitatively reproduces the measured spectrum in that there is a significant spectral extension of up to >4.5 μm. Besides the SC spectra, the simulations also revealed the temporal dynamics of the SCG in different dielectrics. Pulses in the anomalous GVD regime i.e., in CaF_2 and BaF_2, which are shown in Figs. 4(a) and 4(b), are strongly localized near $t = 0$ with short-time scale pulse-splitting. The pulse splitting is due to the plasma generated by the high intensity pulses. This is highly consistent with the measured results in Figs. 3(h) and 3(k). On the contrary, pulse broadening and pulse splitting are clearly observed in the normal GVD regime in ZnS [19], as shown in Fig. 4(c). The spatially averaged autocorrelation traces over the entire spectral bandwidth were simulated for comparison with the measurement results. For the SC in CaF_2, the autocorrelation trace in Fig. 4(d) shows a 17 fs in FWHM, corresponding to a ~12 fs pulse width. This tallies well with the measured self-compressed sub-two-cycle pulse from the SC in CaF_2, except that the measured pulse duration is longer because of the limited phase-matching bandwidth in the SHG FROG measurement. The imperfect self-compression

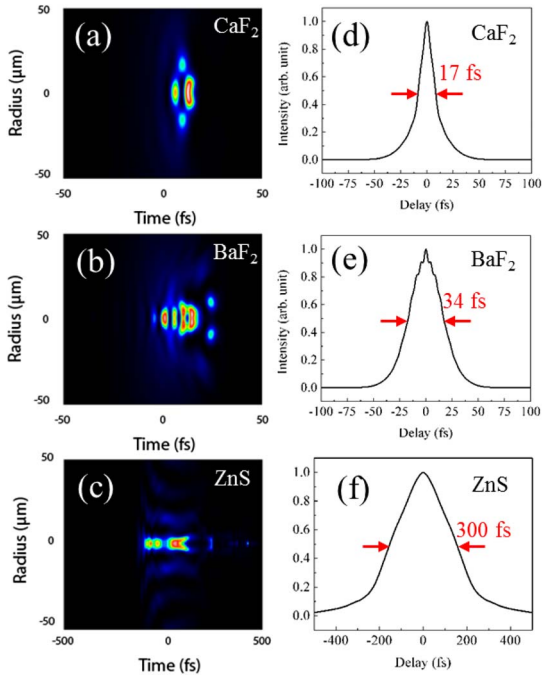

Fig. 4. Simulated spatio-temporal profiles when 2.1 μm, 30 fs pulses pass through (a) CaF_2, (b) BaF_2, (c) and ZnS. 10-times larger time scale is used in (c). Simulated spatially averaged autocorrelation traces of SC in (d) CaF_2, (e) BaF_2, and (f) ZnS. The pulse energies used for simulation are 6 μJ for CaF_2 and BaF_2, and 5 μJ for ZnS.

in BaF_2 is also well reproduced by the simulations shown in Fig. 4(e), with 34 fs FWHM of the autocorrelation trace, corresponding to ~24 fs FWHM pulse width. On the other hand, ZnS broadens the autocorrelation to ~300 fs due to the normal GVD and pulse splitting, which is also consistent with the experimental observation.

In conclusion, we systematically investigated the mid-IR SCG from filaments in bulk dielectrics with normal and anomalous GVD. A three-octave-spanning SC spectrum in ZnS with a normal GVD was generated with a robust and stable output power. In the anomalous GVD regime, the sub-two-cycle self-compression of mid-IR filaments from CaF_2 was experimentally observed. The generated filaments have several micro joules of pulse energy. Such a coherent broadband source with few-cycle duration in the mid-IR range is a promising seed source for seeding mid-IR OPA and OPCPA. It is also a good candidate for time-resolved tools for molecular motion study.

The authors would like to thank Dr. Jeffrey Moses for providing the mid-IR spectrometer. This work was supported by AFOSR (FA9550-12-1-0499 and FA9550-14-1-0255), the Center for Free-Electron Laser Science, DESY, Hamburg, Germany, and the excellence cluster "The Hamburg Centre for Ultrafast Imaging—Structure, Dynamics and Control of Matter at the Atomic Scale" of the Deutsche Forschungsgemeinschaft. H. K. Liang acknowledges the financial support of the Singapore Institute of Manufacturing Technology (SIMT/14-110023) and the Agency for Science, Technology and Research (A*STAR) in Singapore. R. Grynko, D. Weerawarne, and B. Shim acknowledge the financial support of the SUNY Research Foundation. O. Novak acknowledges the support from the European Regional Development Fund, the European Social Fund, and the state budget of the Czech Republic (project HiLASE: CZ.1.05/2.1.00/01.0027, DPSSLasers: CZ.1.07/2.3.00/20.0143, Postdok: CZ.1.07/2.3.00/30.0057). His current affiliation is with the HiLASE Centre, Institute of Physics ASCR, Czech Republic. C.-L. Chang acknowledges the Ministry of Science and Technology in Taiwan for their support via the Postdoctoral Research Abroad Program NSC 102-2917-I-564-026.

References

1. R. R. Alfano, *The Supercontinuum Laser Source* (Springer, 1989).
2. P. Domachuk, N. A. Wolchover, M. Cronin-Golomb, A. Wang, A. K. George, C. M. B. Cordeiro, J. C. Knight, and F. G. Omenetto, Opt. Express **16**, 7161 (2008).
3. G. Qin, X. Yan, C. Kito, M. Liao, C. Chaudhari, T. Suzuki, and Y. Ohishi, Appl. Phys. Lett. **95**, 161103 (2009).
4. C. Xia, M. Kumar, O. P. Kulkarni, M. N. Islam, J. F. L. Terry, M. J. Freeman, M. Poulain, and G. Mazé, Opt. Lett. **31**, 2553 (2006).
5. W. Yang, B. Zhang, G. Xue, K. Yin, and J. Hou, Opt. Lett. **39**, 1849 (2014).
6. C. P. Hauri, R. B. Lopez-Martens, C. I. Blaga, K. D. Schultz, J. Cryan, R. Chirla, P. Colosimo, G. Doumy, A. M. March, C. Roedig, E. Sistrunk, J. Wheeler, L. F. DiMauro, and E. P. Power, Opt. Lett. **32**, 868 (2007).
7. C. R. Petersen, U. Møller, I. Kubat, B. Zhou, S. Dupont, J. Ramsay, T. Benson, S. Sujecki, N. Abdel-Moneim, Z. Tang, D. Furniss, A. Seddon, and O. Bang, Nat. Photonics **8**, 830 (2014).
8. F. Silva, D. R. Austin, A. Thai, M. Baudisch, M. Hemmer, D. Faccio, A. Couairon, and J. Biegert, Nat. Commun. **3**, 807 (2012).
9. J. Darginavicius, D. Majus, V. Jukna, N. Garejev, G. Valiulis, A. Couairon, and A. Dubietis, Opt. Express **21**, 25210 (2013).
10. M. Durand, A. Houard, K. Lim, A. Durecu, O. Vasseur, and M. Richardson, Opt. Express **22**, 5852 (2014).
11. S. V. Chekalin, V. O. Kompanets, E. O. Smetanina, and V. P. Kandidov, Quantum Electron. **43**, 326 (2013).
12. M. Durand, A. Jarnac, A. Houard, Y. Liu, S. Grabielle, N. Forget, A. Durecu, A. Couairon, and A. Mysyrowicz, Phys. Rev. Lett. **110**, 115003 (2013).
13. M. Hemmer, M. Baudisch, A. Thai, A. Couairon, and J. Biegert, Opt. Express **21**, 28095 (2013).
14. A. Couairon and A. Mysyrowicz, Phys. Rep. **441**, 47 (2007).
15. A. Dergachev, Proc. SPIE **8599**, 85990B (2013).
16. J. Moses, S.-W. Huang, K.-H. Hong, O. D. Mücke, E. L. Falcão-Filho, A. Benedick, F. Ö. Ilday, A. Dergachev, J. A. Bolger, B. J. Eggleton, and F. X. Kärtner, Opt. Lett. **34**, 1639 (2009).
17. A. L. Gaeta, Phys. Rev. Lett. **84**, 3582 (2000).
18. B. Shim, S. E. Schrauth, and A. L. Gaeta, Opt. Express **19**, 9118 (2011).
19. J. K. Ranka, R. W. Schirmer, and A. L. Gaeta, Phys. Rev. Lett. **77**, 3783 (1996).